Impact perforation of monolithic polyethylene plates: Projectile nose shape dependence

CrossMark

I. Mohagheghian, G.J. McShane[*], W.J. Stronge

Department of Engineering, University of Cambridge, Trumpington Street, Cambridge CB2 1PZ, UK

ABSTRACT

Ductile thermoplastics, for example Ultra High Molecular Weight Polyethylene (UHMWPE), are of interest for their impact energy absorbing capabilities. While the impact perforation mechanisms of metallic targets have been investigated in some detail, far less progress has been made towards understanding the impact resistance of ductile polymers. The aim of this investigation is to identify the relationship between the projectile tip geometry and impact energy absorption of semi-crystalline thermoplastics. The focus of the study is light-weight monolithic plates of extruded polymer impacted normally by rigid projectiles at velocities up to 100 ms^{-1}. Three polymers will be considered: Low Density Polyethylene (LDPE), High Density Polyethylene (HDPE) and Ultra High Molecular Weight Polyethylene (UHMWPE). Polyethylene provides a convenient test material, as variations in microstructure provide a contrast in mechanical properties, without significant variations in density. Three distinct projectile nose shapes are considered: blunt, hemi-spherical and conical. For a conical tip, perforation occurs by ductile hole expansion. For this nose shape the high yield strength and strain rate sensitivity of HDPE offers an advantage over the other two polyethylenes. Perforation by blunt and hemi-spherical projectiles is more sensitive to deformation localisation. The high strain hardening of UHMWPE, which increases with strain rate, results in a significantly greater impact resistance than either HDPE or LDPE. The perforation mechanisms and energy absorption of these PE plates are contrasted with those of thin aluminium alloy targets that have the same total mass. UHMWPE outperforms these metallic targets for all three projectile nose shapes. Finally, the influence of target thickness on the impact perforation of LDPE is considered. All three nose shapes show a linear increase in perforation energy with target thickness.

© 2015 The Authors. Published by Elsevier Ltd. This is an open access article under the CC BY license (http://creativecommons.org/licenses/by/4.0/).

1. Introduction

Polymers are finding an increasing number of applications in lightweight impact energy absorbing structures. Factors such as low cost, ease of production, corrosion resistance and low density make them an attractive choice. In automotive construction, the dynamic deformation of polymers is an important consideration in vehicle crashworthiness. The low velocity impact energy absorbing characteristics of polymers has been exploited in safety equipment and component packaging. At higher strain rates, polymers are beginning to be considered in defence applications for blast resistance, spall containment and impact damage mitigation.

This investigation focuses on the impact perforation of thin ductile polymer plates by a rigid projectile. While the performance of ductile polymers subjected to lower velocity impacts has been investigated [1–3], far less progress has been made on characterising their performance under higher velocity impacts where perforation can occur. This is in contrast to metallic targets, for which the impact perforation regimes have been investigated in some detail [4–7]. One exception is transparent polymers such as polycarbonate (PC), which have found applications in impact resistant glazing. While PC is mainly used for its optical transparency, studies by Radin & Goldsmith [8] and Wright et al. [9] suggest that it can perform better than equivalent weight metallic targets when subjected to high velocity impacts. Promising results have also been reported recently in the application of elastomers as protective coatings against perforation by fragment impacts [10]. Retrofitting structures with elastomeric coatings has been proposed as a cheap and easy solution for increasing the

* Corresponding author. Tel.: +44 (0)1223 332635.
E-mail address: gjm31@cam.ac.uk (G.J. McShane).

protection against fragmentation caused by blast or impact which can be a major cause of injuries [10,11]. However, there is currently a lack of understanding of the optimal specification for a ductile polymer used as a protective layer for impact perforation resistance, and whether this specification is sensitive to the projectile geometry.

Key to optimising polymer selection for impact resistance is to understand the link between mechanical properties, deformation mechanisms and failure. The morphology of polymers has been reported to have a direct influence on their impact strength. Increasing the degree of crystallinity [12–14] or the size of the spherulites (e. g. in the case of HDPE [15]) is believed to have a negative effect on the impact performance. On the other hand increasing molecular weight generally increases the impact strength [12,16]. Brough et al. [17] studied the impact response of three high density polyethylenes with different molecular weights. The fracture surface of the specimens after Charpy impact testing was studied using Scanning Electron Microscopy (SEM). For low and medium molecular weights, the fracture surface includes numerous rounded nodules, interpreted as a sign of separation of micro-fibrils due to extreme thermal softening. For polymers with ultra high molecular weight the deformation is found to be less localised with no sign of melting processes. A similar observation was reported by Li et al. [18], where the impact strength of high density polyethylene with different molecular weights was studied. Izod tests and SEM were used to evaluate the impact performance. Li et al. [18] found that increasing the molecular weight enhances the resistance to crack propagation and suppresses both brittle fracture modes and thermal softening effects.

It is also well established that strong coupling exists between the thermal and mechanical behaviour of polymers. This coupling becomes more significant at higher rates of deformation where adiabatic heating can result in significant thermal softening. The proportion of mechanical work which is converted to heat (b) has been a topic of much interest and has been found to depend on the polymer type. Garg et al. [19] compared the temperature rise in polycarbonate (PC) and a thermoset epoxy (EPON 862/W) measured with an infrared detector at low and high strain rates. They found that much more energy is stored in epoxy compared to polycarbonate. The greater stored energy was also found to be consistent with greater elastic recovery upon unloading for the epoxy. It was suggested that the ratio of dissipative to total work is greatly dependent on strain and strain rate, and it increases at higher strain rates [19]. Different values of b have been deduced for polyethylene. While $b \approx 1$ is assumed for HDPE [20,21], a much smaller value $b < 0.5$ is identified for UHMWPE [21].

The objective of the present investigation is to develop an understanding of the connection between the mechanical properties of semi-crystalline thermoplastics, and their response to impact by rigid projectiles with different tip geometries. We select polyethylene (PE) as a convenient and versatile family of test materials for this investigation. Three variants are considered here: low density (LDPE), high density (HDPE) and ultra high molecular weight (UHMWPE). The differences in the microstructure of these three polyethylenes provides contrasting mechanical properties, with a relatively small influence on their density, thus controlling the number of variable parameters in the experiments. While the crystalline structure of low density polyethylene (LDPE) and high density polyethylene (HDPE) is in the form of spherulites [22,23], a ribbon-like form is reported for UHMWPE [24]. The yield strength of polyethylene is dependent on the crystalline structure, increasing if either the degree of crystallinity or the lamellar thickness increases [25,26]. The degree of crystallinity is reported to be highest for HDPE followed by UHMWPE and LDPE [27,28]. While in the early stages of deformation (small strains) the material

response is mainly governed by the crystalline regions in the microstructure, they soon become fragmented and reoriented as deformation progresses. The later stages of deformation in polyethylene, as well as other semi-crystalline polymers, is mainly controlled by the amorphous phase and can be well represented by theories adapted from rubber elasticity [29,30]. For UHMWPE, physical entanglement of polymer chains causes strong strain hardening, a consequence of the high molecular weight. The effect of chain entanglement on plastic deformation of LDPE and UHMWPE was investigated by Bartczak [31,32]. It was found that by increasing the density of entanglements in the amorphous phase, the rate of strain hardening increases and the strain at the onset of hardening decreases.

In this investigation, the modes of deformation and failure of the polymers will be investigated, and the sensitivity to projectile nose shape will be considered. To support the interpretation of the impact tests, quasi-static perforation of the plates will also be considered, allowing a detailed assessment of the perforation mechanisms in the absence of inertia and strain-rate effects. Results for the perforation of monolithic metallic plates (aluminium alloy 6082) are also provided, to allow the deformation and failure modes and energy absorbing capabilities of the two material classes to be compared. Finally, the influence of plate thickness on the nose-shape sensitivity of impact perforation is evaluated.

The paper is structured as follows. In Section 2, polymer characterisation tests are reported, covering different modes of deformation and a range of strain rates. The quasi-static and impact perforation experiments on polymer plates are reported in Sections 3 and 4, respectively. An evaluation of plate thickness dependence is presented in Section 5. Conclusions are given in Section 6.

2. Polymer characterisation

Throughout this investigation, commercially supplied extruded polyethylene sheets are used. With the exception of Section 5, the sheet thickness used for all tests described here are 2.9 mm for the HDPE, 3.0 mm for the LDPE and 3.0 mm for the UHMWPE. In this section the extruded polyethylene sheets are characterised in order to support the interpretation of the indenter perforation experiments described subsequently. Three characterisation methodologies are considered: the viscoelastic properties are determined using dynamic mechanical analysis (DMA), and the elastic–plastic behaviour is identified under both uniaxial tension and shear.

2.1. Dynamic mechanical analysis

Dynamic mechanical analysis (DMA) was performed on the extruded polyethylene specimens to gain some insight into the microstructure and small strain mechanical properties. A Triton TT-DMA test machine was used, with the specimen mounted in a cantilever beam configuration with fully clamped boundary conditions at the tips. Beam specimens with total length 40 mm and width 11.85 mm were machined from the polymer sheets and clamped in the machine such that the free length of cantilever in bending was 12.7 mm. The thickness of the beams were the same as the extruded sheet. The tests were conducted in sinusoidal bending at a frequency of 1 Hz and tip amplitude of 0.02 mm over a range of temperatures. To achieve this, the chamber containing the specimen was first cooled using liquid nitrogen to a starting temperature of −175 °C, before commencing controlled heating at a rate of 5 °C/min using the test machine's furnace. The results are shown in Fig. 1.

Polyethylenes have been shown to demonstrate three peaks in loss modulus with increasing temperature, corresponding to relaxation mechanisms referred to as α, β and γ [33–35]. The β and
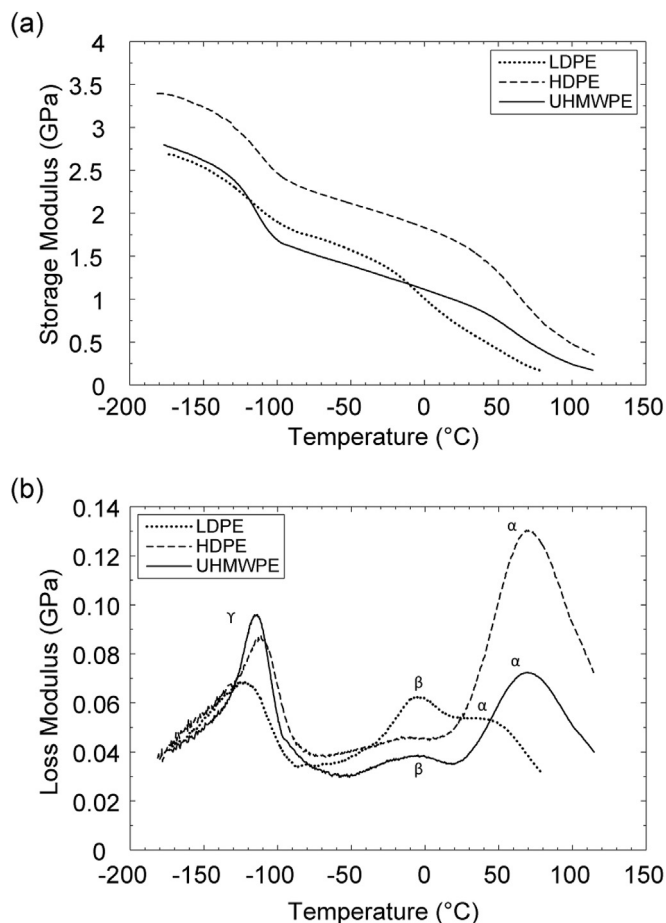
(a)

(b)

Fig. 1. DMA results for LDPE, HDPE and UHMWPE: temperature scan at a beam bending frequency of 1 Hz. (a) Storage modulus and (b) loss modulus.

γ relaxations are related to molecular chain motion in the amorphous phase and the α relaxation is attributed to chain motion in the crystalline phase. While the magnitude of the β peak is observed to decrease with increasing crystallinity [33], the α peak temperature is reported to increase linearly with the degree of crystallinity and the crystallite dimensions [35]. The γ relaxation is normally taken to define the glass transition temperature [35]. The α, β and γ transitions are marked in Fig. 1b for the three polyethylenes. Comparing α and β peaks indicates that HDPE has the highest degree of crystallinity and the LDPE the least. The relaxation characteristics of UHMWPE are more similar to those of HDPE than LDPE. All three show a γ relaxation at around −120 °C, indicating similar glass transition temperatures.

2.2. Tensile tests

Tensile tests were conducted on dog-bone shaped specimens according to ASTM D638 (type V). The gauge section has length 9.5 mm and width 3.2 mm. The thickness of each sample is the same as the extruded sheets. Dog-bone specimens were machined from the sheets in two directions, parallel and perpendicular to the extrusion direction, in order to assess the anisotropy of the material. To evaluate the strain rate sensitivity of the polymers, tensile tests at nominal strain rates of 10^{-2}, 10^{-1} and 10^0 s^{-1} were performed. Tensile tests were carried out using an Instron screw driven test machine, at approximately constant cross-head velocity. The nominal stress was calculated from the Instron load cell

measurements, and nominal strain was obtained using the cross head displacement.[1]

The tensile responses of LDPE, HDPE and UHMWPE at two strain rates are plotted in Fig. 2. Consider first the results at a nominal strain rate of 10^{-2} s^{-1} (Fig. 2a). The HDPE shows the highest yield strength, and LDPE the lowest. The higher yield strength of HDPE is consistent with its higher crystallinity. In contrast, UHMWPE shows a higher degree of strain hardening, which can be attributed to greater physical entanglement of polymer chains in the amorphous phase [31,36]. All of the polymers show a drop in nominal stress after yielding. This drop is most significant for HDPE. Neck formation and propagation occurs in the LDPE and HDPE specimens after this drop. In contrast no sign of necking is observed in the UHMWPE specimen, a result of the stabilising effect of the higher strain hardening. On completion of neck propagation, strain hardening increases in the LDPE and HDPE samples. The failed samples are shown in Fig. 3b-d. HDPE shows the highest tensile ductility at a nominal strain rate of 10^{-2} s^{-1}. The key uniaxial tensile properties are summarised in Table 1.

Fig. 2b shows the tensile response at an increased nominal strain rate of 10^0 s^{-1}. Both LDPE and HDPE now fail during the neck propagation phase. As can be seen in Fig. 3e-f, HDPE fails immediately after neck formation, whereas LDPE fails after the neck propagates to some extent. Failure during neck propagation has been reported by many researchers during higher strain rate tests [20,37,38]. Thermal softening caused by adiabatic heating has been suggested as a reason for destabilising the neck and leading to failure [20,37,39]. It was argued by Hillmansen & Haward [20] that for medium and high density polyethylene adiabatic heating starts becoming significant for strain rates in the range 10^{-2}–10^0 s^{-1}. It should be mentioned that material inside the neck can experience strain rates an order of magnitude higher than regions outside the neck [40] (A similar phenomenon has also been observed in metallic specimens [41]). For UHMWPE at a strain rate of 10^0 s^{-1}, the load drops slightly after the yield point, but strain hardening begins almost immediately. The stabilising effect of this strain hardening permits continued tensile deformation (Fig. 3g), and consequently UHMWPE has the highest tensile ductility at this strain rate. The failure strain results for the three polymers are summarised in Table 1. Repeat measurements of failure strain show a larger variability than observed for the yield strength.

Note also that the degree of strain hardening increases with strain rate for nominal strains below 300%. This phenomenon has also been reported for UHMWPE by Mourad et al. [42] for tensile tests at strain rates of 10^{-2}–10^3 s^{-1} and by Brown et al. [43] in compression at strain rates in the range 10^{-4}–10^3 s^{-1}. In contrast Brown et al. [43] observed no increase in strain hardening with strain rate for HDPE for the range of strain rates studied. For UHMWPE, a reduction in strain hardening is observed for nominal strains above 300% at the strain rate of 10^0 s^{-1} (Fig. 2b). This reduction in the rate of strain hardening was also reported by Gorwade et al. [44] and Furmanski et al. [21] and attributed to thermal softening. Thermal imaging performed by Gorwade et al. [44] shows a rise of nearly 40 °C during quasi-static tensile tests on UHMWPE, for a strain rate of 2×10^{-1} s^{-1}. Furmanski et al. [21] argued that for UHMWPE, there is a deviation from isothermal conditions due to adiabatic heating after 15% of strain, leading to significant softening at larger strains. In the current tensile

---

[1] The experimental method used in this investigation did not allow the local measurement of true stress, true strain and true strain rate after the onset of necking, at which point the deformation becomes highly non-uniform. Hence, nominal stress, nominal strain and nominal strain rate are used to characterise the overall response of these ductile polymers to large deformations.
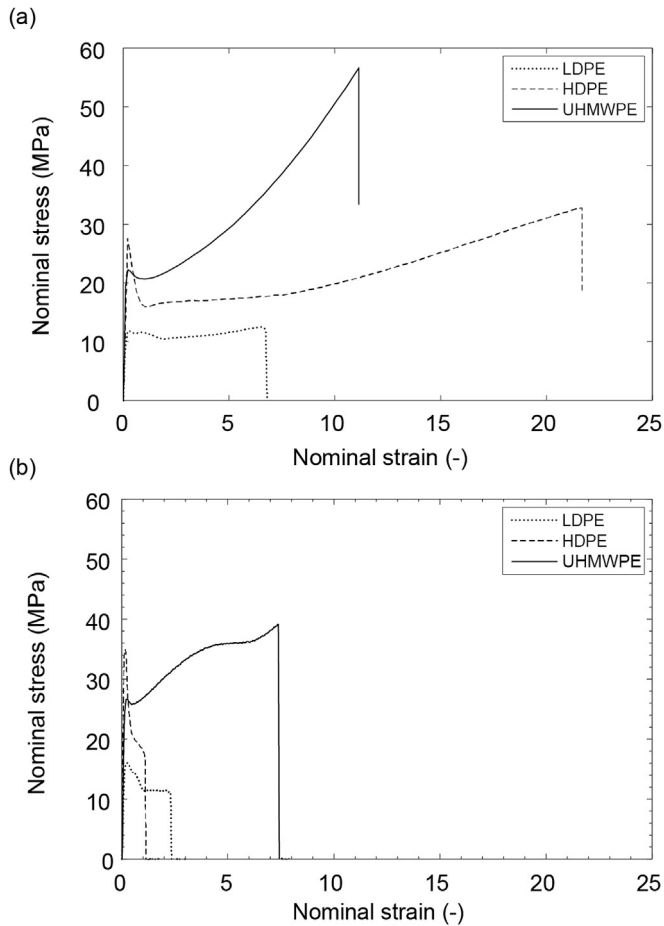
(a)

(b)

Fig. 2. Uniaxial tensile response of LDPE, HDPE and UHMWPE at nominal strain rates of (a) 10^{-2} s^{-1} and (b) 1 s^{-1}.

experiments, although no temperature measurement were performed, touching the specimen immediately after failure indicated that considerable heating had occurred in the sample.

The effect of strain rate on the yield stress is summarised in Fig. 4a. Three repeat tests were performed for each data point,
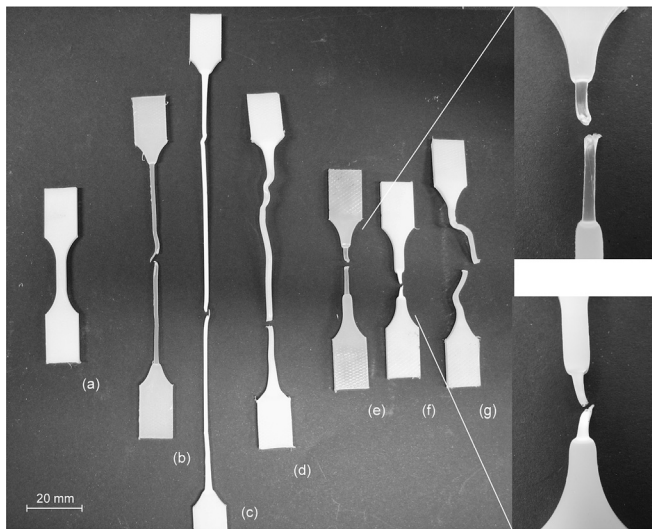

Fig. 3. Photographs of tensile test specimens: (a) untested dogbone specimen, (b) LDPE (10^{-2} s^{-1}), (c) HDPE (10^{-2} s^{-1}), (d) UHMWPE (10^{-2} s^{-1}), (e) LDPE (1 s^{-1}), (f) HDPE (1 s^{-1}) and (g) UHMWPE (1 s^{-1}).

showing excellent repeatability (the error bars in Fig. 4b show the spread of the measured values). It should be mentioned that the yield stress is defined here as the maximum stress recorded before the first drop in stress occurs (Fig. 2). While the strain rate sensitivity of HDPE is highest, there is little difference between LDPE and UHMWPE. The range of strain rates considered here is well below those corresponding to sub-ordinance projectile impacts (of the order 10^3–10^4 s^{-1}). However, it has been shown that the linear dependency of yield stress with log strain rate extends to strain rates of the order 10^8 s^{-1} at room temperature for HDPE and UHMWPE [21,45,46]. The explanation is provided by Mulliken & Boyce [47]. It is shown that this linear trend persists as long as only one relaxation mechanism influences the plastic deformation. For all three polymers at room temperature and low strain rates, this will be the α relaxation (Fig. 1b). As the strain rate is increased, the β relaxation may begin to have an influence. However, the β peak is only significant for the LDPE (Fig. 1b). For all three polymers (LDPE, HDPE and UHMWPE), the temperature of the γ relaxation is sufficiently low that this mechanism is unlikely to influence deformation at sub-ordinance impact velocities.

The anisotropy of the extruded polymer sheets is shown in Fig. 4b, comparing the yield strength measured from dog-bones machined in two perpendicular directions in the plane of the extruded sheet. The average and range of repeat tests are shown, again indicating excellent repeatability. HDPE shows the highest anisotropy, although this is small. No significant anisotropy is seen for LDPE and UHMWPE.

2.3. Shear tests

A series of shear tests were conducted on the polyethylene samples at strain rates spanning five orders of magnitude (10^{-3}–10^1 s^{-1}). Tests were conducted following the procedure outlined in ASTM standard D 732. Polymer plates with the same thickness as the extruded sheets were clamped between steel confinement plates, through which a circular cylindrical steel punch (itself clamped to the specimen) was driven, subjecting the polymer to shear deformation at the punch perimeter. The lower strain rate tests (10^{-3}–10^0 s^{-1}) were performed using an Instron screw driven test machine, with the punch placed in contact with the cross head and load cell of the machine. A servo-hydraulic test machine was used for the higher rate test (10^1 s^{-1}). In order to achieve a constant punch velocity during the loading of the sample at the higher strain rate, it was necessary to leave a small gap between the punch and cross head at the start of the test to allow the cross head to accelerate before making contact. A thin layer of rubber was placed between the two surfaces in order to dampen possible vibrations caused by the impact between the cross head and the punch.

The shear test results for LDPE, HDPE and UHMWPE are shown in Fig. 5. At a strain rate of 10^{-3} s^{-1} HDPE shows nearly no strain hardening post yielding. The degree of strain hardening is higher for the LDPE and significantly higher for the UHMWPE. Similar behaviour was reported by Gul [48] for these three polymers. The yield strength of all three polymers increases with shear strain rate. For HDPE, pronounced softening is observed as the strain rate is increased. Softening of HDPE in shear was also reported at strain rates exceeding 3×10^{-2} s^{-1} by G'Sell et al. [49]. They attributed this to thermal softening. For LDPE this softening begins only at higher strain rates, in excess of 10^1 s^{-1} (Fig. 5a). For UHMWPE not only can no sign of softening be seen for the range of strain rates covered by these experiments, but the degree of strain hardening continues to increase with increasing strain rate (Fig. 5c).

Table 1
Uniaxial tensile properties of the polyethylene and Al alloy specimens used in the current investigation. Yield strength and nominal failure strain are provided at the strain rates indicated. The range of measured values are quoted alongside the mean.

Material	Yield strength (MPa)			Nominal failure strain (−)		
	0.01 s^{-1}	0.1 s^{-1}	1 s^{-1}	0.01 s^{-1}	0.1 s^{-1}	1 s^{-1}
LDPE	11.9 ± 0.3%	13.3 ± 1.5%	16.3 ± 2.2%	7.2 ± 5.7%	8.9 ± 3.5%	2.1 ± 11%
HDPE	27.6 ± 1.0%	31.3 ± 1.5%	35.2 ± 0.8%	21.7 ± 0.2%	14.0 ± 18%	1.1 ± 4.8%
UHMWPE	22.0 ± 1.3%	23.9 ± 0.3%	26.4 ± 1.0%	10.1 ± 10%	8.7 ± 16%	6.6 ± 14%
AA 6082 T4	171.2	–	–	0.23	–	–
AA 6082 T6	302.4	–	–	0.16	–	–

3. Quasi-static perforation of monolithic PE plates

In this section, the perforation of polyethylene plates is investigated under quasi-static indentation loading using three different indenter nose shapes. The test configuration is chosen to mirror that of the impact experiments described subsequently. The objective is to support the interpretation of the modes of deformation and perforation of the polymers, by first reducing the influence of any inertia and strain rate effects. The quasi-static indentation tests also allow more precise measurement of the indentation force and displacement than is possible during an impact experiment.

3.1. Test configuration

The test specimens used in this investigation consist of flat plates with a circular test area fully clamped around the edge at a radius $R = 50$ mm. The specimen thickness is equal to the extruded sheet thickness: 2.9 mm for HDPE and 3.0 mm for both LDPE and UHMWPE specimens. The boundary constraint is provided by a circular steel clamping ring with inner diameter 100 mm, as shown in Fig. 6. Twelve M4 bolts are used to fasten the clamping ring through clearance holes in the test specimen (a square plate of side length 130 mm) to a supporting plate. Axisymmetric indenters with three distinct nose shapes are used, including blunt, hemi-spherical and conical, each with a diameter of 12.5 mm. The ratio of indenter to plate radius is therefore $R_i/R = 0.125$. The indenters are machined from mild steel, and undergo no plastic deformation during the indentation experiments.

The quasi-static perforation experiments were performed using an Instron screw driven test machine. The indenters were mounted to the load cell on the cross-head of the machine, with the specimen and clamping plate supported beneath. The load cell was used to record the indentation force, and the cross-head displacement provided the indenter displacement. All of the indentation tests were conducted at a rate of 1 mm min^{-1}. The tests were stopped after the indenter had fully perforated the plate.

3.2. Quasi-static indentation results

Fig. 7a shows the variation in indentation force with displacement for a blunt indenter. The response can be divided into two stages: before and after the onset of localisation. Before the onset of localisation the whole plate contributes to carrying the load through elastic and plastic bending and stretching. At the point marked by a cross in Fig. 7a, deformation localises at the perimeter of the indenter. The onset of localisation corresponds to the peak in the indenter force−displacement plot. The material in this zone then draws out, and can reach high levels of strain before finally failing. This drawing of the material is evident in the failed samples, shown in Fig. 8.

The higher elastic modulus and yield strength of HDPE results in larger indenter forces during the first stage of deformation.

However, the onset of localisation occurs much sooner in HDPE than the other polymers. This can be explained by the absence of strain hardening observed for HDPE in the quasi-static shear characterisation experiments, Fig. 5 (the onset of localisation occurs within a zone of intense shearing at the perimeter of the indenter). After localisation, during the drawing phase, the state of stress in the material in this region becomes predominantly tensile. The drawing phase persists longer for the HDPE than the other two polymers, as is evident in Fig. 8 and the indenter displacement recorded in this second phase of deformation (Fig. 7). This is consistent with the greater tensile ductility of HDPE at low strain rates, shown in Fig. 2. Liu & Piggott [50] also concluded that tensile, rather than shear, failure dominates the final stages of shear punch indentation of ductile polymers. Despite the greater tensile ductility of HDPE compared to LDPE, both fail at the same total indenter displacement, due to the earlier onset of localisation in the
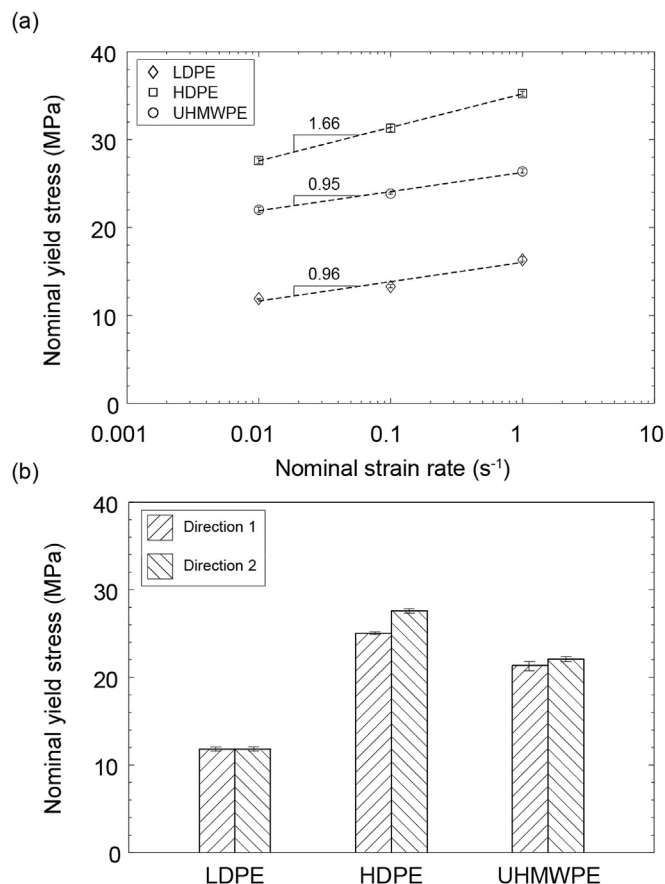

Fig. 4. (a) Variation in yield strength with strain rate and (b) yield strength at a strain rate of 10^{-2} s^{-1} in two orthogonal directions in the plane of the extruded sheet for LDPE, HDPE and UHMWPE.
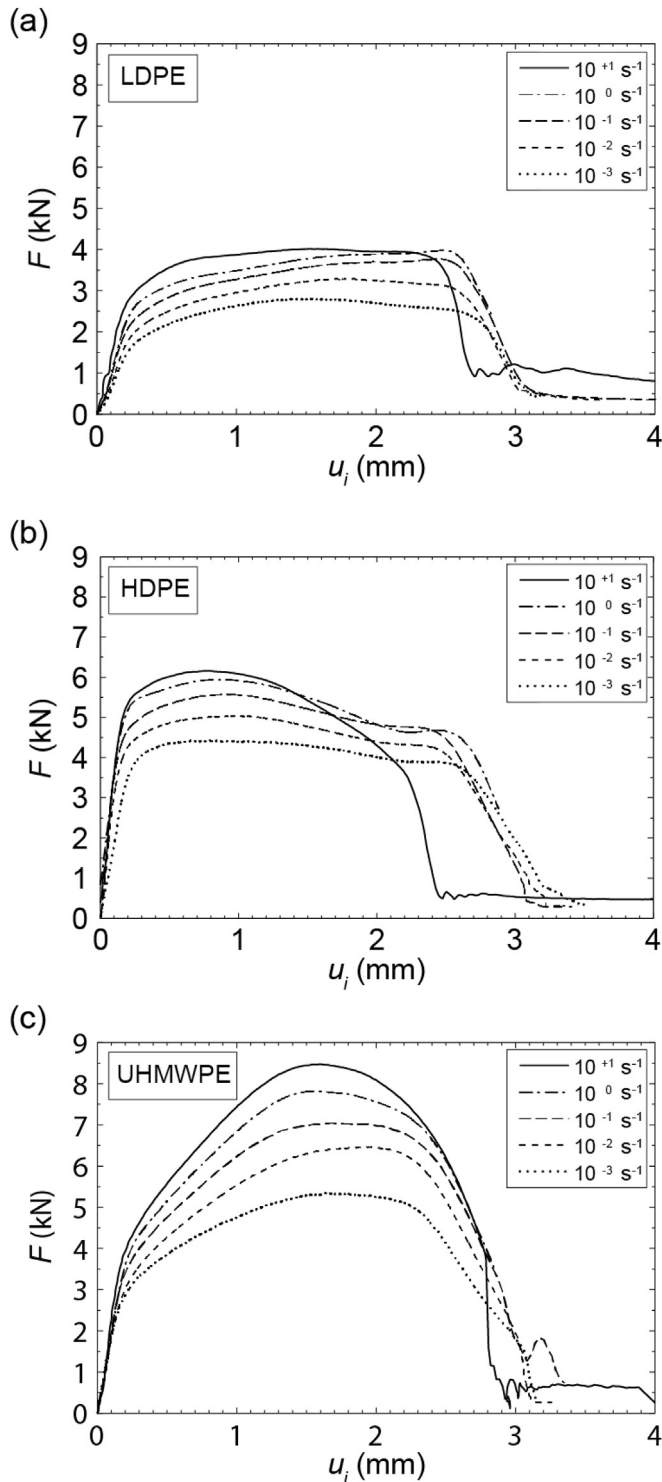
Fig. 5. Shear punch test results for (a) LDPE, (b) HDPE and (c) UHMWPE for strain rates spanning five orders of magnitude: 10^{-3}–10 s^{-1}.

Fig. 6. Plate clamping arrangement and indenter geometries.

HDPE. For UHMWPE, localisation occurs at larger indenter displacements than the other two polymers. This allows a much greater total energy absorption. This resistance to shear localisation at the perimeter of the blunt indenter can be attributed to the higher strain hardening measured for UHMWPE under shear deformation (Fig. 5).

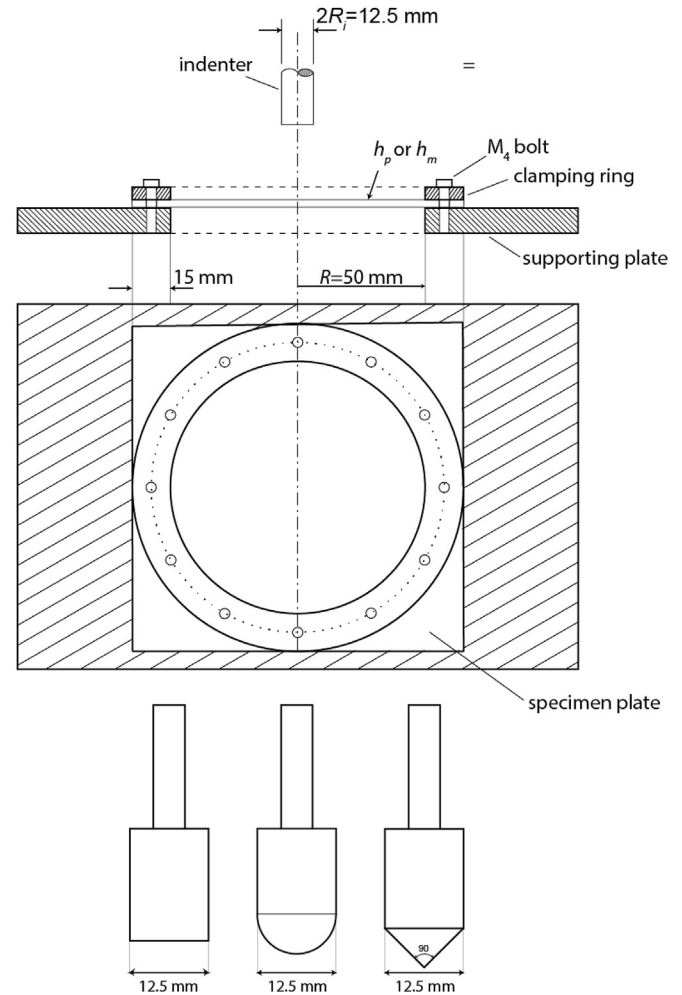Similar stages of deformation can be observed for the hemispherical indenter: global plate bending and stretching, localisation, drawing and failure (Fig. 7b). The slope of the indenter force-displacement curve before localisation is generally lower than for the blunt indenter. This is consistent with a smaller contact patch size [51]. The indenter displacements at the onset of localisation are similar to the blunt indenter, occurring first for the HDPE, followed by LDPE and UHMWPE. However, the subsequent drawing phase continues to much larger indenter displacements for the hemi-spherical indenter compared with the blunt. This is evident in significant thinning of the polymer at the indenter tip (Fig. 8). Again, the drawing phase is most extensive for HDPE, consistent with its higher quasi-static tensile ductility. The influence of its greater strain hardening is apparent during the drawing phase for UHMWPE.

For the conical indenter, a different sequence of deformation and failure is observed. For the LDPE and HDPE specimens failure is initiated by the formation of a small hole at the indenter tip, which expands as indentation progresses until the indenter passes through the plate completely. The force does not fall to zero after full perforation due to frictional resistance, the contact pressure between the plate and the indenter being affected by the elastic contribution to hole expansion. The significant elastic strains present during perforation are shown in Fig. 8: note that the final diameter of the holes after elastic recovery are significantly smaller than the projectile diameter, particularly for LDPE. The failure mechanism is different in the case of UHMWPE. Failure begins with the formation of a single crack in the material. Perforation of the
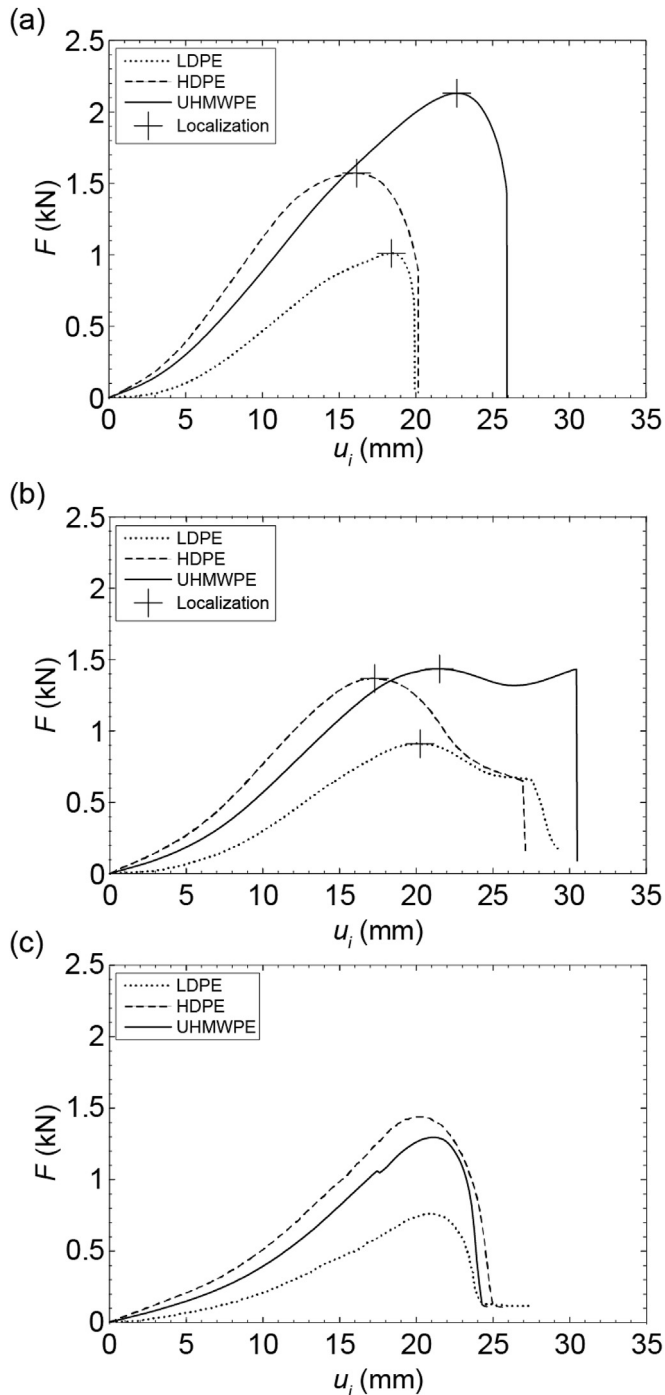
(a)

(b)

(c)

Fig. 7. Quasi-static indentation response of LDPE, HDPE and UHMWPE plates using (a) blunt, (b) hemi-spherical and (c) conical indenters. The tests were performed at an indentation speed of 1 mm min^{-1}. The markers indicate the onset of localisation.

plate is preceded by the propagation of this crack followed by bending of two petals until the indenter is able to pass through. The indenter displacement at full perforation is insensitive to the polymer choice, as it depends only on expansion of the hole to a critical size, which is a function predominantly of projectile diameter and tip angle. However, the resistance to penetration (by elastic–plastic hole expansion) prior to full perforation increases with the initial yield strength of the polymer (Table 1). The high degree of strain hardening of UHMWPE does not appear to play a

significant role. As a result, the total perforation energy is greatest for HDPE for a conical indenter. The quasi-static perforation energies are summarised in Table 2.

4. Impact perforation of monolithic PE plates

In this section the response of the monolithic plates to impact loading will be investigated. The objective is to assess the modes of deformation, failure and energy absorption under dynamic loading for the three different nose shapes and draw comparisons with perforation under quasi-static loading.

4.1. Impact test methodology

The target dimensions and clamping arrangements used in the impact experiments were identical to those described above for the quasi-static tests and illustrated in Fig. 6. The polymer test specimens were also identical to those described in Section 3. Projectiles with diameter 12.5 mm (identical to the indenter geometry used in the quasi-static experiments) and mass 20.2 ± 0.2 g were machined from mild steel. It should be noted that for each tip geometry, the length of the projectile was adjusted slightly so as to ensure the same total mass. No plastic deformation of the projectiles was observed during any of the impact experiments. The projectile was fired using a gas gun with barrel of internal diameter 12.7 mm. The specimen supporting plate was mounted to a steel frame and oriented normal to the barrel, so that the projectile impacted at 90° to the target. A high speed camera (Vision Research Phantom V710) oriented perpendicular to the flight of the projectile was used to record the motion of the projectile during its interaction with the target. The projectile was designed with a tail of diameter 5 mm and length 20 mm, in which reference grooves were machined, so that the high speed camera could continue to track the projectile motion throughout its interaction with the target, even when the nose was obscured by the clamping frame. The high speed images therefore provided measurements of both the impact velocity V_i and the residual velocity V_r. Positive velocity is defined in the direction of initial impact, so that a negative V_r indicates reflection of the projectile, and a positive V_r indicates perforation. Laser velocity gauges mounted at the barrel exit were used to verify the impact velocity obtained from the high speed photography, and showed good agreement.

A measure of the ballistic limit for each target was obtained by plotting residual velocity V_r against impact velocity V_i for a number of impact experiments. A curve was fitted through all data points with $V_r \geq 0$. The intersection of this curve with the zero residual velocity axis is considered to be the ballistic limit V_{bl} in this investigation. A polynomial form for the curve fit was used, based on the Lambert and Jonas relation [52]:

$$V_r = a\left(V_i^p - V_{bl}^p\right)^{1/p} \tag{1}$$

where a, p and V_{bl} are fitting parameters. To ensure adequate resolution of V_{bl}, repeat experiments were conducted near to the ballistic limit in order to achieve at least 4 data points within ±4 ms^{-1} of V_{bl}.

4.2. Failure modes

The failure modes of polyethylene plates under impact loading are shown in Fig. 9 for the three different nose shapes. For the hemi-spherical nose shape, it can be seen that the tensile drawing phase, after the onset of localisation, is significantly reduced for impact loading. Instead, for the LDPE and HDPE plates, a polymer
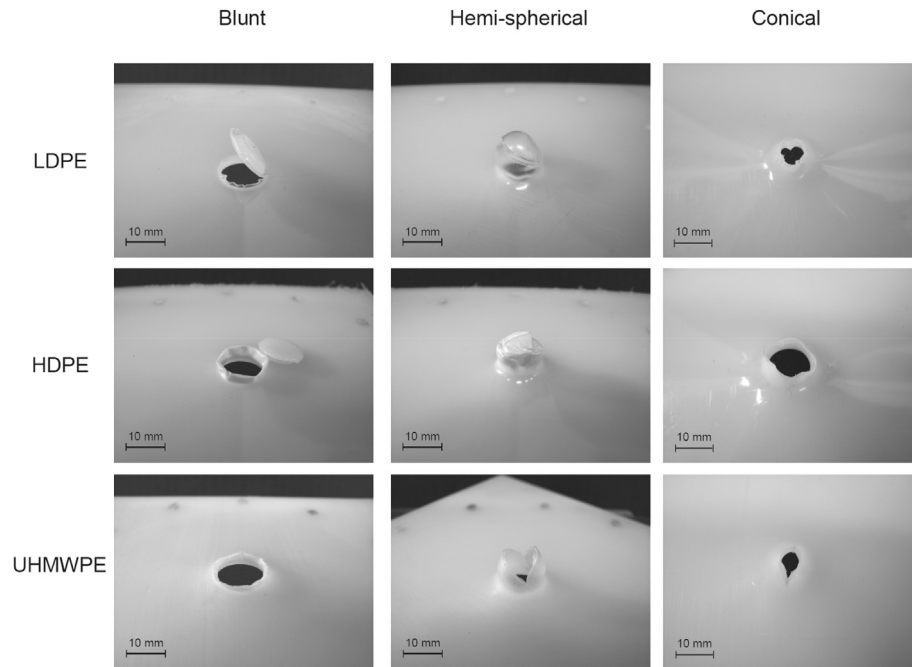
Fig. 8. Quasi-static perforation mechanisms for LDPE, HDPE and UHMWPE plates using blunt, hemi-spherical and conical indenters.

cap detaches at the tip of the projectile. This is consistent with the reduced tensile ductility of these materials at increased strain rates (Fig. 2b). For UHMWPE a cap does not form. Instead, the failure occurs by radial cracking and the formation of petals (Fig. 9). This polymer undergoes a high degree of strain hardening at higher strain rates (Fig. 2b), which resists localisation. The impact failure modes for the blunt and conical projectiles, which feature less tensile stretching, are similar to the quasi-static cases.

4.3. Impact energy absorption

Impact results for the LDPE targets are shown in Fig. 10 for the three projectile nose shapes. Fig. 10a, c and e compare the residual velocity of the projectile with the impact velocity. Best fit lines to the residual velocity based on the Lambert–Jonas relationship (equation (1)) are shown, and the fitting coefficients, including the ballistic limit, are listed in Table 3. Fig. 10b, d and f show the kinetic energy loss of the projectile, ΔE, which gives a measure of the energy absorbed by the target:

$$\Delta E = \frac{1}{2} m \left(V_i^2 - V_r^2 \right).$$ (2)

Table 2
Summary of the quasi-static and dynamic perforation energies for different target materials and nose shapes. The polyethylene results are for plates of thickness 3 mm. The Al alloy results are for plates of thickness 1 mm.

Material	Perforation energy (J)					
	Blunt nose shape		Hemi-spherical nose shape		Conical nose shape	
	Quasi-static	Dynamic	Quasi-static	Dynamic	Quasi-static	Dynamic
LDPE	9.5	20.9	14.0	32.2	8.4	30.0
HDPE	19.0	25.0	21.6	38.0	17.9	33.2
UHMWPE	30.5	58.3	27.4	66.3	14.7	30.6
AA 6082 T4	12.2	38.8	28.7	65.5	18.6	21.4
AA 6082 T6	14.9	32.8	35.4	47.4	16.5	22.3

here m is the mass of the projectile. Three guidelines are also provided. The first, given by the dotted line, corresponds to the initial kinetic energy of the projectile. The other two, the dashed and dashed-dotted lines, are obtained by substituting the Lambert–Jonas relationship (1) into equation (2), with the fitting parameters as given in Table 3. We define the impact perforation energy E_p to be the value of ΔE at the ballistic limit:

$$E_p = \frac{1}{2} m V_{bl}^2.$$ (3)

The impact results for the three projectile nose shapes and three polymer types are summarised in Fig. 11. The quasi-static results are also shown for comparison. Perforation energy values are given in Table 2. Consider first the blunt nose shape, Fig. 11a. For all three polymer types, the perforation energy under impact loading is higher than for quasi-static perforation. The largest increase can be seen for UHMWPE, and the lowest for HDPE, despite the latter having the highest strain rate sensitivity of the yield strength (Refer to Fig. 4a, noting that the linear trends in yield strength with log strain rate can be expected to extend to the higher strain rates experienced during the impact tests, as discussed in Section 2.2). This indicates that a high degree of strain hardening, which delays the localisation, and a resistance to softening post-localisation play a more important role in the resistance to impact perforation by a blunt projectile than the yield strength of the polymer. Similar behaviour is observed for the hemi-spherical projectile (Fig. 11b). However, the dynamic elevation in perforation energy is greater for this nose shape compared to the blunt, for all three polymers. This mode of perforation, which does not exhibit the same severity of deformation localisation as seen at the perimeter of the blunt projectile, therefore appears to be less sensitive to the thermal softening experienced by HDPE and LDPE. However, a high degree of strain hardening, which persists and increases at high strain rates, continues to result in a performance benefit for UHMWPE under impact conditions. For a conical projectile, the increase in perforation energy due to dynamic loading is similar for all three polymer types. For this perforation mechanism (predominantly elastic and plastic hole expansion), the elastic modulus and yield
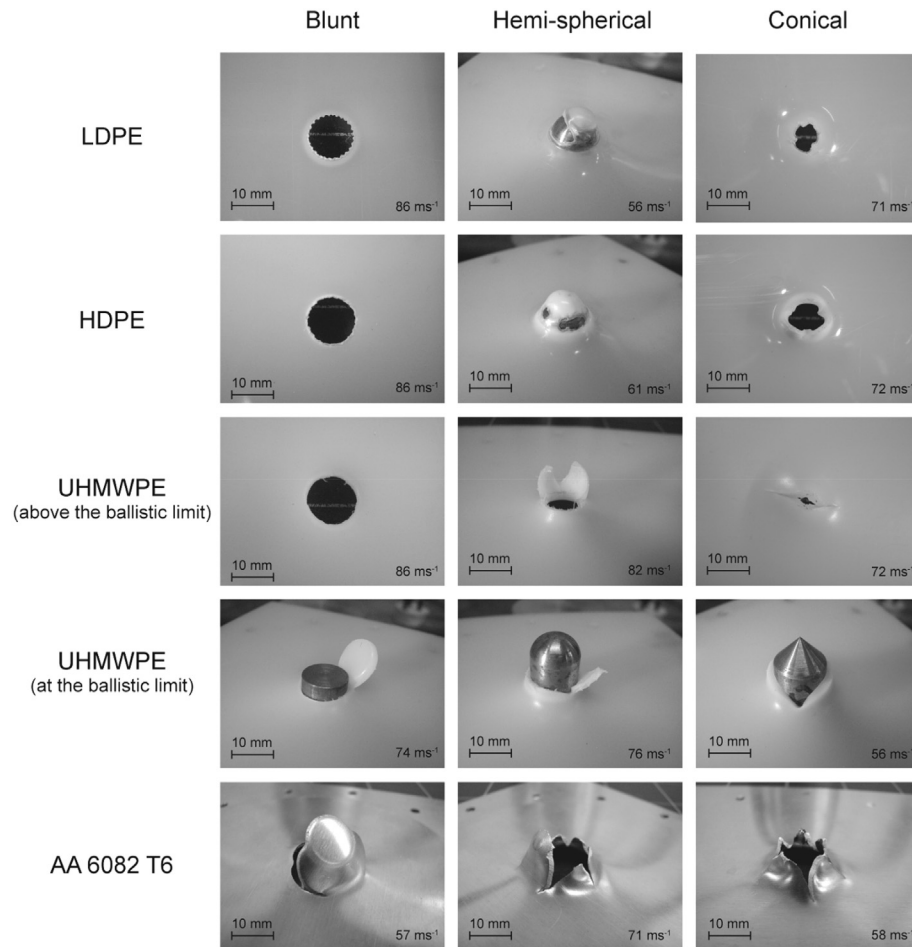
Fig. 9. Impact perforation mechanisms for LDPE, HDPE and UHMWPE plates using blunt, hemi-spherical and conical projectiles. Results are also shown for aluminium alloy 6082-T6 plates of the same weight.

strength are more important than the resistance to deformation localisation. Consequently, the performance gain offered by UHMWPE against blunt and hemi-spherical projectiles is lost, and HDPE provides the greatest perforation resistance.

4.4. Comparison with the impact response of lightweight metallic plates

In this section, the impact response of the three polymers is compared with that of a typical structural light alloy, aluminium alloy 6082. The aim is to identify similarities and differences between the perforation characteristics of these two classes of lightweight construction materials under impact loads. The competitiveness of these polymers for impact energy absorbing applications can thus be assessed. Two tempers of AA 6082 are considered, T4 and T6, providing a contrast in mechanical properties without altering the density, in an analogous fashion to the PE specimens. Aluminium alloy sheet of thickness 1 mm is used, giving the targets approximately the same mass per unit area as the 3 mm thick polyethylene specimens.

In order to characterise the two alloy tempers, quasi-static tensile tests were conducted according to the standard ASTM-E8. Dog-bone specimens with gauge length 32 mm and width 6 mm were machined from the aluminium alloy sheet. The specimens were loaded to failure in an Instron screw driven test machine. A laser extensometer was used to measure the strains in this case. The

applied force was again obtained from the test machine load cell. The results are plotted in Fig. 12. Alloy 6082-T6 has a higher yield strength but lower tensile ductility and lower strain hardening compared to the T4 temper.

The impact perforation mechanisms of 6082-T6 are compared with the LDPE, HDPE and UHMWPE plates of the same weight in Fig. 9. For a blunt projectile, the metallic plate fails in the region of local shear deformation at the perimeter of the projectile, similar to the polymer cases. Whereas deformation then proceeds in the LDPE and HDPE cases by tensile drawing of material at the projectile perimeter, the metallic plate fails by the propagation of two radial cracks. For the hemi-spherical projectile, the mode of failure again begins in a similar manner for metal and polymer targets, with the formation of a cap at the tip of the projectile due to deformation localisation. However, in the metallic case, this is again accompanied by radial cracking. For the conical projectile, the metal plate fails by a petalling mode (radial cracking initiated by tip perforation), as opposed to the ductile hole enlargement seen for the LDPE and HDPE cases. It is notable that for all three projectile nose shapes, the failure mode of the UHMWPE is intermediate between the aluminium alloy and the other two polymers, sharing characteristics of both. In particular, radial cracking occurs for UHMWPE, though to a lesser extent than the metallic specimens.

The energy absorption and residual velocity curves for aluminium alloy 6082-T6 targets are compared with the equivalent weight LDPE plates in Fig. 10. For the metallic target, the energy
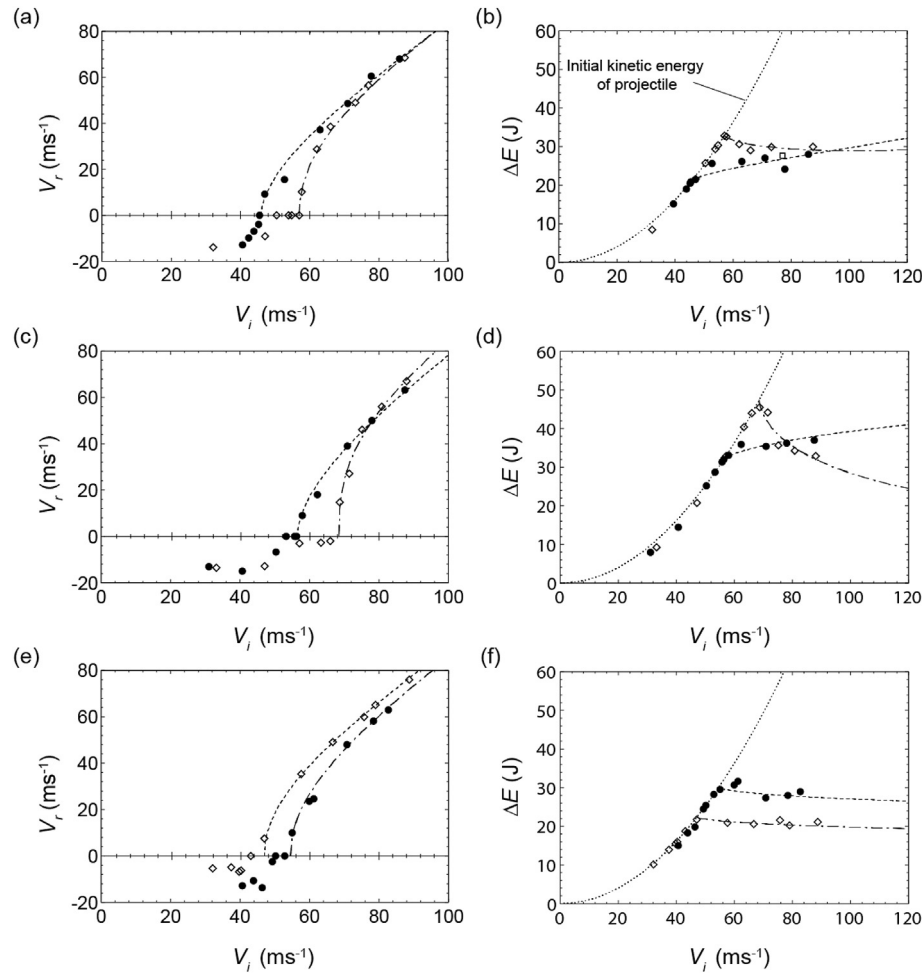
Fig. 10. Projectile residual velocity and energy absorption versus impact velocity for (a-b) blunt, (c-d) hemi-spherical and (e-f) conical projectiles. Solid and hollow symbols represent 3 mm thickness LDPE and 1 mm thickness AA 6082 T6 targets respectively.

absorption ΔE increases up to the ballistic limit and then decreases for impact velocities above the ballistic limit. This fall in ΔE post-perforation has been reported for metallic targets by a number of researchers [4–7]. An important mechanism in this fall is a reduction in the amount of plastic 'dishing' deformation as the impact velocity increases beyond the ballistic limit [4]. Teng & Wierzbicki [6] also argue that a transition in the local failure mode from tensile tearing to shear failure at higher impact velocities contributes to this fall for a round nosed projectile. A similar trend in ΔE is seen for LDPE impacted by a conical projectile. However, for the other two nose shapes, the polymer plates show increasing ΔE post-perforation. A key difference between the LDPE and aluminium alloy targets is the strong strain rate sensitivity of the polymer. This may explain the additional dissipation at higher impact velocities for the blunt and hemi-spherical projectiles, whose failure modes both involve large, localised plastic straining in the LDPE case.

In Fig. 13, the ballistic limits of the 3 mm polyethylene plates (LDPE, HDPE and UHMWPE) are compared with the 1 mm thick aluminium alloy plates in (both T6 and T4 tempers). Depending on the projectile nose shape, the highest perforation resistance can be achieved either by a metal or a polymer target. For a conical nose shape, all three polymers outperform both aluminium alloy targets. The ductile hole enlargement perforation mechanism dissipates more energy than the petalling mode, despite the much lower yield strength of the polymers. The higher yield strength of HDPE gives it an advantage over the other two polymers. For the blunt and hemi-spherical projectiles, the UHMWPE outperforms both metallic alloys, due to the resistance to deformation localisation provided by its high degree of strain hardening. However, LDPE and HDPE, with their susceptibility to softening at high strain rates, both underperform the metallic plates for these tip geometries.

5. Effect of polymer plate thickness

The experimental results have so far focussed on polymer plates of thickness 3 mm. In this section the effect of increasing the plate thickness on the perforation resistance and failure modes is considered for LDPE targets. Plates of thickness 3.0, 4.5, 5.9 and 9.1 mm are impacted by projectiles with blunt, hemi-spherical and
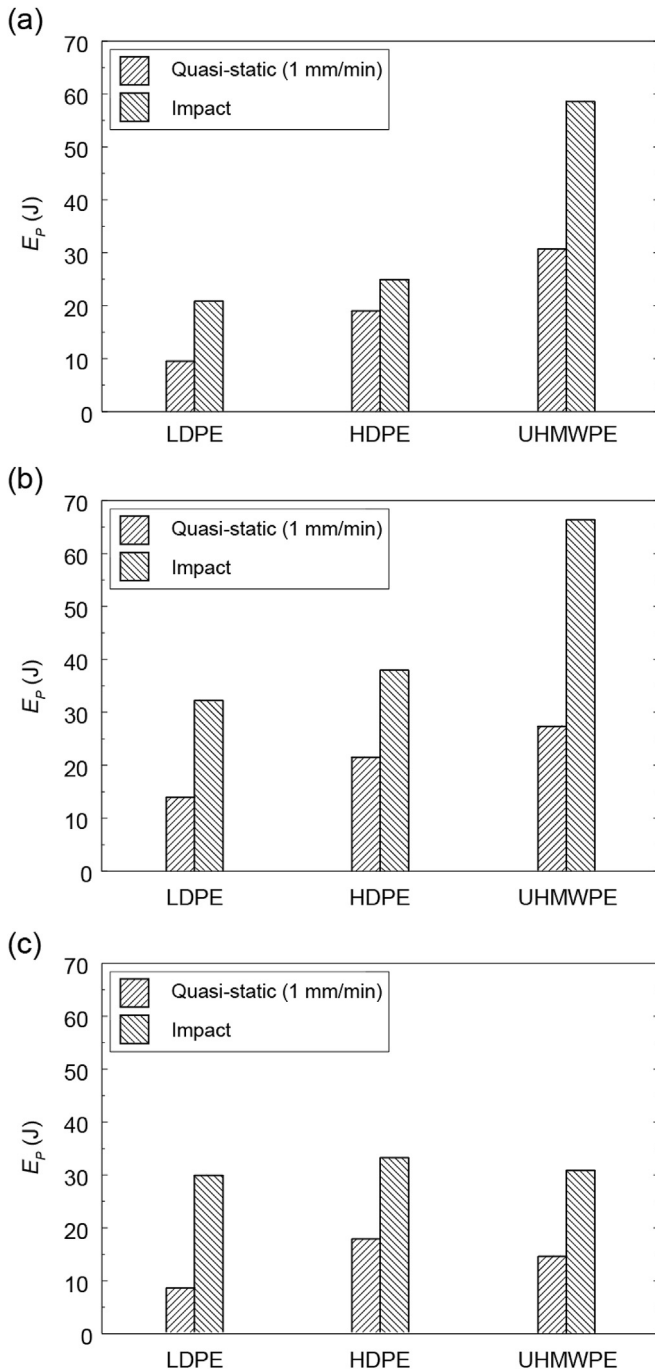
Table 3
Fitting coefficients for the Lambert–Jonas relationship, equation (1), for the target materials and plate thicknesses indicated.

Projectile nose shape	LDPE (thickness 3 mm)			AA 6082 T6 (thickness 1 mm)		
	V_{bl} (ms^{-1})	a	p	V_{bl} (ms^{-1})	a	p
Blunt	45.5	0.98	1.80	57.0	0.98	2.22
Hemi-spherical	56.5	1	1.80	68.5	1	2.70
Conical	54.5	1	2.10	47.0	1	2.10

(a)

(b)

(c)

Fig. 11. Comparison between perforation energy under quasi-static indentation and impact for (a) blunt, (b) hemi-spherical and (c) conical indenters.

Fig. 12. Uniaxial tensile response of AA 6082 in two tempers: T6 and T4.

Fig. 13. Comparison between the impact resistance of three types of PE and Al alloy 6082 in two tempers (T6 and T4) with the same plate mass.

the other two nose shapes. A similar trend has been reported for metals [5,8,53] and for polycarbonate [8,9]. For these materials, the trend is the result of a trade-off between a reduction in plastic deformation of the whole plate, through global bending and stretching, and an increase in localised plastic deformation at the

Fig. 14. Perforation energy versus plate mass per unit area for LDPE plates impacted by projectiles with three different nose shapes.

conical nose shapes, using an identical impact test methodology to that described in Section 4. For each target thickness, residual velocity curves were used to identify the ballistic limit and perforation energy, as described previously for the 3 mm plates.

The results are summarised in Fig. 14. It can be seen that the perforation energy (E_p) increases linearly with increasing plate mass for all three nose shapes. The highest perforation energy is obtained for hemi-spherical and conical projectiles, which deliver nearly the same performance over the full range of plate thicknesses considered. For the blunt projectile, both the perforation energy and its rate of increase with plate thickness is lower than for
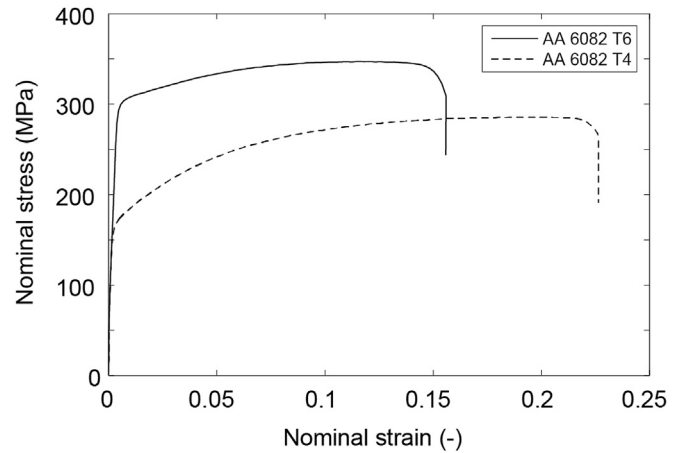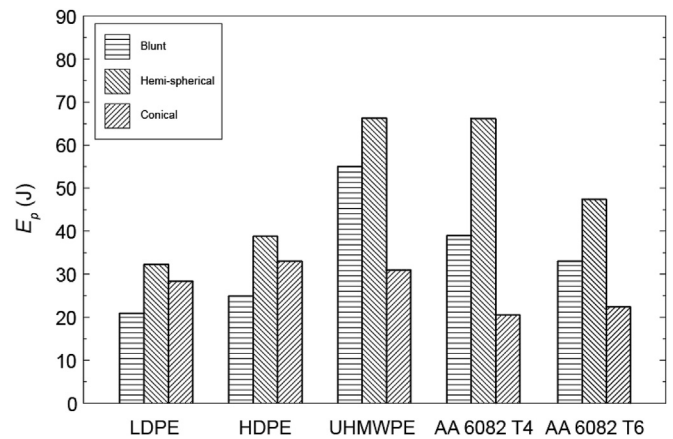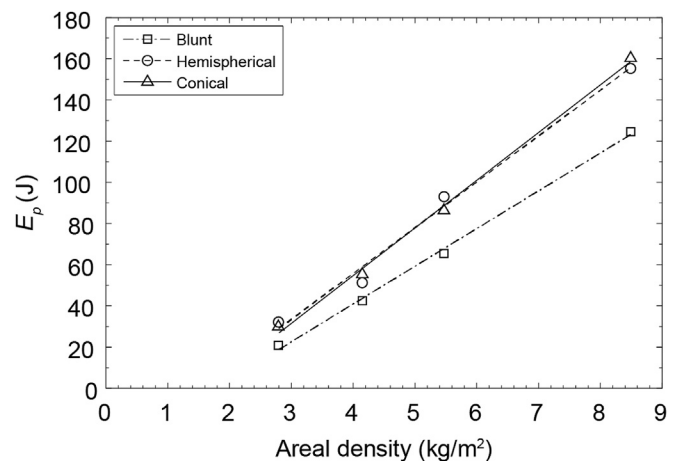
perimeter of the projectile (which is in turn influenced by adiabatic heating and thermal softening). The LDPE targets tested here undergo a similar localisation in deformation as the thickness is increased. Figs. 15—17 show diametral sections through a 9.1 mm thick LDPE plate impacted by blunt, hemi-spherical and conical projectiles, respectively, at the velocities indicated. Dashed lines are added to the figures to highlight the edge of the hole in the plate. The results show that the characteristics of the deformation localisation are dependent on the projectile nose shape, as follows.

For the blunt projectile, indentation occurs on the proximal surface of the plate, across the projectile contact patch. However, significant stretching deformation also occurs beneath the projectile at the distal surface (Fig. 15a). At the ballistic limit (Fig. 15b), a polymer cap is detached showing two regions of deformation: a cylindrical portion (where the cap ultimately detaches from the plate), and a domed section due to the stretching deformation at the distal face (Fig. 15c). Closer examination of the rough, cylindrical section of the plug using Scanning Electron Microscopy (Fig. 15d and e) reveals a significant amount of fibrillation, which is indicative of tensile failure (the failure surface is distinct from that observed for the shear characterisation experiments, Section 2). A degree of tensile drawing of material in the target plate at the perimeter of the projectile is also evident in Fig. 15b.

The mode of deformation is different for the hemi-spherical projectile (Fig. 16). In this case, there is more extensive drawing out of the polymer at the tip of the projectile. The degree of drawing
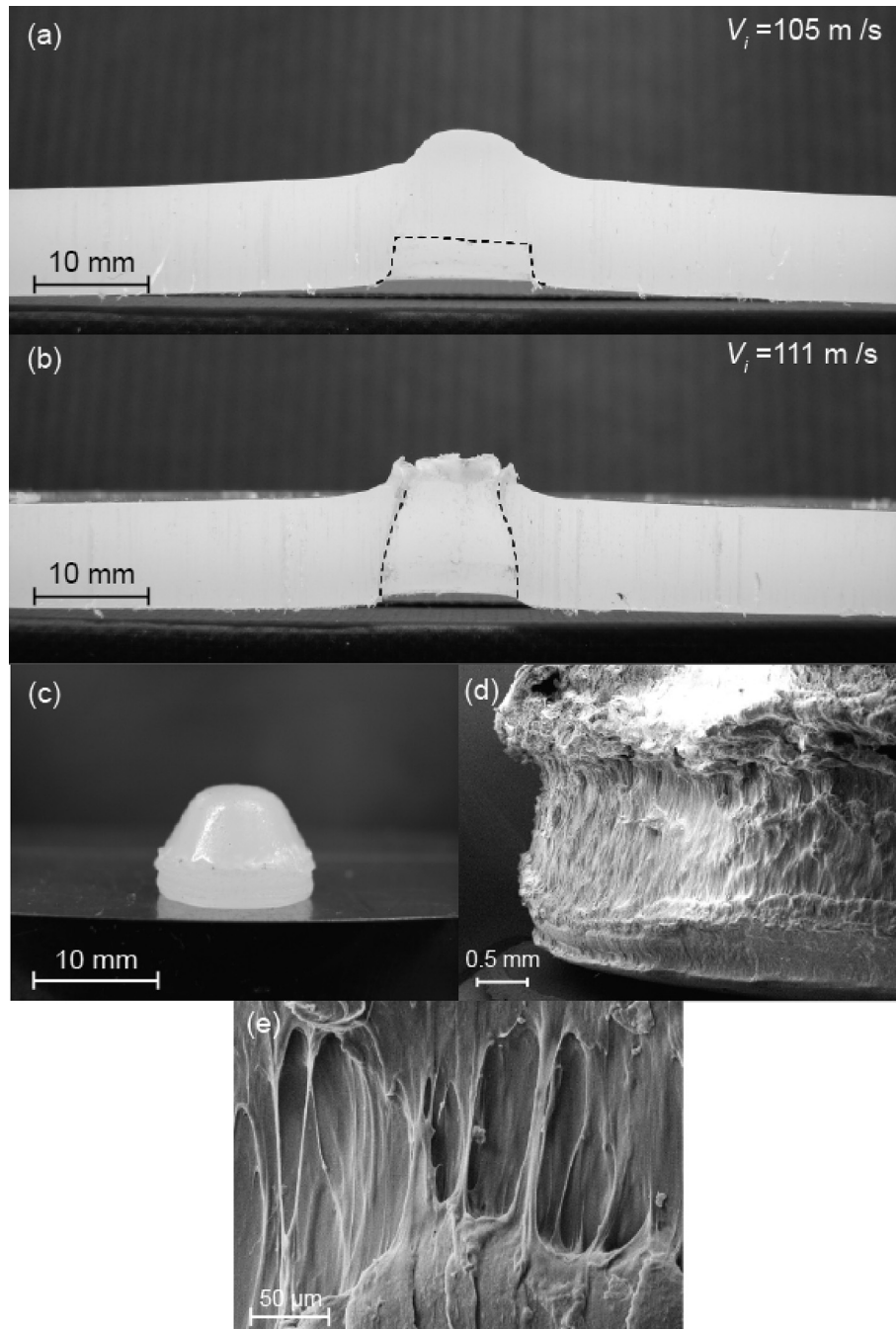

Fig. 15. Deformation and perforation of 9.1 mm thick LDPE plates by a blunt projectile: (a-b) diametral sections for the impact velocities indicated, (c) the plug formed at the tip of the projectile, (d-e) SEM micrographs of the surface of the plug.
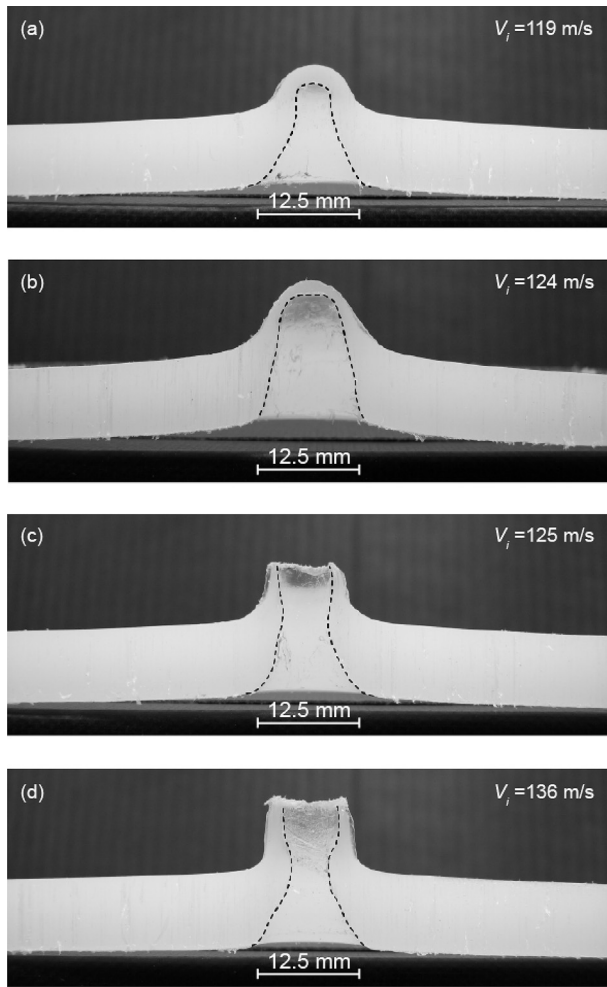
Fig. 16. Deformation and perforation of 9.1 mm thick LDPE plates by a hemi-spherical projectile: diametral sections for the impact velocities indicated. The scale bar shows the projectile diameter.

Fig. 17. Deformation and perforation of 9.1 mm LDPE plates by a conical projectile: (a-b) diametral sections for the impact velocities indicated, with a scale bar showing the projectile diameter. (c-d) Show the perforated plate close to the ballistic limit.

achieved prior to full perforation by the projectile increases with the impact velocity (Fig. 16c and d). In contrast to the thinner target plates (Fig. 9) no cap detachment is observed at the tip of the projectile for the thick LDPE target. The 'hourglass' shape of the cavity left by the projectile is a result of elastic recovery − the projectile diameter (12.5 mm) is marked on Fig. 16. Considering the perforation energy (Fig. 14), the more extensive tensile drawing achieved by the hemi-spherical projectile compared to the blunt results in a greater perforation resistance as the plate thickness is increased.

The perforation of a thick plate by a conical projectile is shown in Fig. 17. Around the ballistic limit, the mechanism of deformation is similar to the hemi-spherical case, showing extensive tensile drawing at the perimeter of the projectile. Unlike the hemi-spherical case, a polymer cap can form and detach at the tip of the conical projectile (Fig. 17c). However, the perforation energy for these two tip geometries is very similar (Fig. 12).

6. Conclusions

The quasi-static and impact perforation of three types of polyethylene (LDPE, HDPE and UHMWPE) is investigated experimentally. Characterisation tests including tensile and shear tests as well as dynamic mechanical analysis have been performed in order to
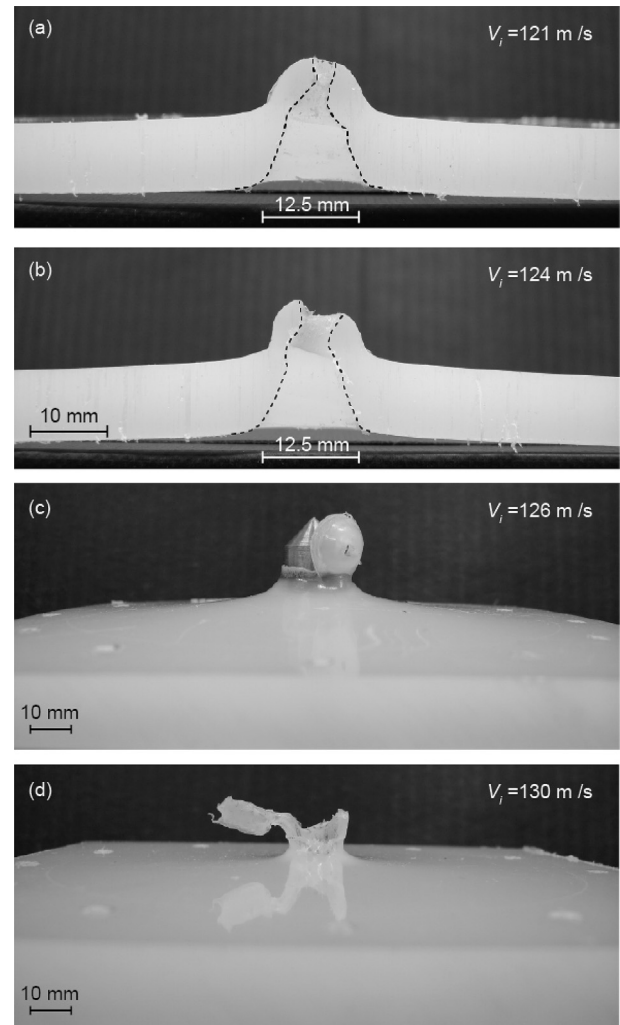
better understand the behaviour of these polymers during impact deformation. The following conclusions are made:

− Tensile and shear test results indicate that for LDPE and HDPE, increasing the strain rate causes softening which, in the case of tensile loading, destabilises neck propagation and leads to premature failure. This kind of softening, which is more significant for HDPE, is believed to occur by adiabatic heating. For UHMWPE, which has a higher level of physical entanglement of polymer molecular chains, not only is there no sign of softening, but also the strain hardening, which has a stabilising effect, increases with increasing strain rate.

− The quasi-static indentation response of polyethylene plates indicates a higher perforation resistance for UHMWPE under both hemi-spherical and blunt indenters. This is due to higher strain hardening, which delays the onset of localisation. This effect is particularly significant for the blunt indenter. The higher stiffness and strength of HDPE leads to a greater indentation resistance prior to localisation, though the earlier onset of localisation limits overall performance. However, this material offers the greatest energy absorption for a conical nose shape, for which elastic−plastic hole expansion is the key perforation mechanism.

— The energy required to perforate the polymer plates is larger for impact loading compared to quasi-static loading. However, the magnitude of the increase depends on both the polymer type and the projectile nose shape. For hemi-spherical and blunt projectiles, UHMWPE shows the greatest increase and HDPE the lowest. HDPE has the highest and most strain rate sensitive yield strength. However, for these projectile nose shapes, resisting localisation and softening during plastic deformation is key. HDPE exhibits the most significant softening at elevated strain rates, and UHMWPE the least, due to a high degree of strain hardening that increases with strain rate. For impact by a conical projectile yield strength again plays the key role in perforation resistance, and the HDPE target performs best.

— The relative impact resistance of polyethylene and two types of aluminium alloy targets of the same weight depends on the projectile nose shape. For blunt and hemi-spherical projectiles, aluminium alloy 6082 in both T4 and T6 tempers outperforms LDPE and HDPE, but underperforms in comparison with UHMWPE. For a conical projectile, all three polymers outperform 6082 aluminium alloy (T4 and T6), with HDPE offering the greatest perforation resistance. This occurs despite the yield strength of the Al alloys being an order of magnitude larger than that of PE.

— The impact perforation resistance of LDPE increases linearly with target thickness for all three projectile nose shapes. The perforation energy for conical and hemi-spherical projectiles is similar, and in excess of that for a blunt projectile, over the full range of plate masses considered. This is due to differences in the perforation mechanisms: significant tensile drawing of the polymer at the projectile perimeter occurs for conical and hemi-spherical projectiles, whereas perforation is by plug formation for the blunt projectile.

Acknowledgements

References

[1] Moura RT, Clausen AH, Fagerholt E, Alves M, Langseth M. Impact on HDPE and PVC plates – experimental tests and numerical simulations. Int J Impact Eng 2010;37:580–98.

[2] Daiyan H, Andreassen E, Grytten F, Lyngstad OV, Luksepp T, Osnes H. Low-velocity impact response of injection-moulded polypropylene plates – part 1: effects of plate thickness, impact velocity and temperature. Polym Test 2010;29:648–57.

[3] Daiyan H, Andreassen E, Grytten F, Lyngstad OV, Luksepp T, Osnes H. Low-velocity impact response of injection-moulded polypropylene plates – part 2: effects of moulding conditions, striker geometry, clamping, surface texture, weld line and paint. Polym Test 2010;29:894–901.

[4] Corran RSJ, Shadbolt PJ, Ruiz C. Impact loading of plates — an experimental investigation. Int J Impact Eng 1983;1:3–22.

[5] Børvik T, Langseth M, Hopperstad OS, Malo KA. Perforation of 12 mm thick steel plates by 20 mm diameter projectiles with flat, hemispherical and conical noses. Int J Impact Eng 2002;27:19–35.

[6] Teng X, Wierzbicki T. Transition of failure modes in round-nosed mass-to-beam impact. Eur J Mech A Solids 2005;24:857–76.

[7] Iqbal MA, Gupta NK. Energy absorption characteristics of aluminum plates subjected to projectile impact. Lat Am J Solids Struct 2008;5:259–87.

[8] Radin J, Goldsmith W. Normal projectile penetration and perforation of layered targets. Int J Impact Eng 1988;7:229–59.

[9] Wright SC, Fleck NA, Stronge WJ. Ballistic impact of polycarbonate—an experimental investigation. Int J Impact Eng 1993;13:1–20.

[10] Porter JR, Dinan RJ, Hammons MI, Knox KJ. Polymer coatings increase blast resistance of existing and temporary structures. AMPTIAC Quarterly 2000.

[11] Davidson JS, Fisher JW, Hammons MI, Porter JR, Dinan RJ. Failure mechanisms of polymer-reinforced concrete masonry walls subjected to blast. J Struct Eng 2005;131:1194–205.

[12] Starkweather HW, Moore GE, Hansen JE, Roder TM, Brooks RE. Effect of crystallinity on the properties of nylons. J Polym Sci 1956;21:189–204.

[13] Van der Wal A, Mulder JJ, Gaymans RJ. Fracture of polypropylene: the effect of crystallinity. Polym Guildf 1998;39:5477–81.

[14] Xu T, Yu J, Jin Z. Effects of crystalline morphology on the impact behavior of polypropylene. Mater Des 2001;22:27–31.

[15] Ohlberg SM, Roth J, Raff RAV. Relationship between impact strength and spherulite growth in linear polyethylene. J Appl Polym Sci 1959;1:114–20.

[16] Karger-kocsis J, Moos E, Mudra I, Varga J. Effects of molecular weight on the perforation impact behavior of injection-molded plaques of α-and β-phase isotactic polypropylenes. J Macromol Sci Part B 1999;38:647–62.

[17] Brough I, Haward RN, Healey G, Wood A. Scanning electron micrographs of high density polyethylene fracture surfaces. Polym Guildf 2004;45:3115–23.

[18] Li B, Gong G, Xie B-H, Yang W, Yang M-B. Influence of molecular weight on impact fracture behavior of injection molded high density polyethylene: scanning electron micrograph observations. J Appl Polym Sci 2008;109:1161–7.

[19] Garg M, Mulliken AD, Boyce MC. Temperature rise in polymeric materials during high rate deformation. J Appl Mech 2008;75:011009.

[20] Hillmansen S, Haward RN. Adiabatic failure in polyethylene. Polym Guildf 2001;42:9301–12.

[21] Furmanski J, Cady CM, Brown EN. Time–temperature equivalence and adiabatic heating at large strains in high density polyethylene and ultrahigh molecular weight polyethylene. Polym Guildf 2013;54:381–90.

[22] Sasaki S, Sakaki Y, Takahara a, Kajiyama T. Microscopic lamellar organization in high-density polyethylene banded spherulites studied by scanning probe microscopy. Polym Guildf 2002;43:3441–6.

[23] Lin Y, Du W, Tu D, Zhong W, Du Q. Space charge distribution and crystalline structure in low density polyethylene (LDPE) blended with high density polyethylene (HDPE). Polym Int 2005;54:465–70.

[24] Gómez-Barrena E, Medel F, Puértolas JA. Polyethylene oxidation in total hip arthroplasty: evolution and new advances. Open Orthop J 2009;3:115–20.

[25] Brooks NW, Ghazali M, Duckett RA, Unwin AP, Ward IM. Effects of morphology on the yield stress of polyethylene. Polym Guildf 1999;40:821–5.

[26] Schrauwen BAG, Janssen RPM, Govaert LE, Meijer HEH. Intrinsic deformation behavior of semicrystalline polymers. Macromolecules 2004;37:6069–78.

[27] Bartczak Z, Lezak E. Evolution of lamellar orientation and crystalline texture of various polyethylenes and ethylene-based copolymers in plane-strain compression. Polym Guildf 2005;46:6050–63.

[28] Chakravartula A, Komvopoulos K. Viscoelastic properties of polymer surfaces investigated by nanoscale dynamic mechanical analysis. Appl Phys Lett 2006;88:131901.

[29] Mills PJ, Hay JN, Hayward RN. The post-yield behaviour of low-density poly-ethylenes. J Mater Sci 1985;20:501–7.

[30] Haward RN. Strain hardening of high density polyethylene. J Polym Sci Part B Polym Phys 2007;45:1090–9.

[31] Bartczak Z. Effect of chain entanglements on plastic deformation behavior of linear polyethylene. Macromolecules 2005;38:7702–13.

[32] Bartczak Z. Effect of chain entanglements on plastic deformation behavior of ultra-high molecular weight polyethylene. J Polym Sci Part B Polym Phys 2010;48:276–85.

[33] Nitta K -h, Tanaka A. Dynamic mechanical properties of metallocene catalyzed linear polyethylenes. Polym Guildf 2001;42:1219–26.

[34] Matsuo M, Bin Y, Xu C, Ma L, Nakaoki T, Suzuki T. Relaxation mechanism in several kinds of polyethylene estimated by dynamic mechanical measurements, positron annihilation, X-ray and 13C solid-state NMR. Polym Guildf 2003;44:4325–40.

[35] Munaro M, Akcelrud L. Correlations between composition and crystallinity of LDPE/HDPE blends. J Polym Res 2008;15:83–8.

[36] Cheng JJ, Alvarado-Contreras JA, Polak MA, Penlidis A. Chain entanglements and mechanical behavior of high density polyethylene. J Eng Mater Technol 2010;132:1–7.

[37] Fager L-O, Bassani JL. Neck propagation in polymers with adiabatic heat generation. Mech Mater 1990;9:183–94.

[38] Dasari A, Misra RDK. On the strain rate sensitivity of high density poly-ethylene and polypropylenes. Mater Sci Eng A 2003;358:356–71.

[39] Vincent PI. The necking and cold-drawing of rigid plastics. Polym Guildf 1960;1:7–19.

[40] Parsons E, Boyce MC, Parks DM. An experimental investigation of the large-strain tensile behavior of neat and rubber-toughened polycarbonate. Polym Guildf 2004;45:2665–84.

[41] Alves M, Jones N. Influence of hydrostatic stress on failure of axisymmetric notched specimens. J Mech Phys Solids 1999;47:643–67.

[42] Mourad A-HI, Elsayed HF, Barton DC, Kenawy M, Abdel-latif LA. Ultra high molecular weight polyethylene deformation and fracture behaviour as a function of high strain rate and triaxial state of stress. Int J Fract 2003;120:501–15.

[43] Brown EN, Willms RB, Gray GT, Rae PJ, Cady CM, Vecchio KS, et al. Influence of molecular conformation on the constitutive response of polyethylene: a comparison of HDPE, UHMWPE, and PEX. Exp Mech 2007;47:381–93.

[44] Gorwade CV, Alghamdi AS, Ashcroft IA, Silberschmidt VV, Song M. Finite element analysis of the high strain rate testing of polymeric materials. J Phys Conf Ser 2012;382:012043.

[45] Briscoe BJ, Nosker RW. The influence of interfacial friction on the deformation of high density polyethylene in a split Hopkinson pressure bar. Wear 1984;95: 241–62.

[46] Walley SM, Field JE. Strain rate sensitivity of polymers in compression from low to high rates. DYMAT J 1994;1:211–27.

[47] Mulliken AD, Boyce MC. Mechanics of the rate-dependent elastic–plastic deformation of glassy polymers from low to high strain rates. Int J Solids Struct 2006;43:1331–56.

[48] Gul R. Improved UHMWPE for use in total joint replacement. Massachusetts Institute of Technology; 1997 [PhD thesis].

[49] G'Sell C, Boni S, Shrivastava S. Application of the plane simple shear test for determination of the plastic behaviour of solid polymers at large strains. J Mater Sci 1983;18:903–18.

[50] Liu K, Piggott MR. Fracture failure processes in polymers. I: mechanical tests and results. Polym Eng Sci 1998;38:60–8.

[51] Onat E, Haythornthwaite R. The load carrying capacity of circular plates at large deflection. J Appl Mech 1954;23:49–55.

[52] Lambert JP, Jonas GH. Towards standardization in terminal ballistics testing: velocity representation. Maryland, USA: USA Ballistic Research Laboratory, Aberdeen Proving Ground; 1976. Report No. 1852.

[53] Dey S, Børvik T, Hopperstad OS, Leinum JR, Langseth M. The effect of target strength on the perforation of steel plates using three different projectile nose shapes. Int J Impact Eng 2004;30:1005–38.